Computationally efficient algorithms for Brownian dynamics simulation of long flexible macromolecules modeled as bead-rod chains

Mahdy Malekzadeh Moghani and Bamin Khomami

Phys. Rev. Fluids **2**, 023303 — Published 17 February 2017

DOI: 10.1103/PhysRevFluids.2.023303

COMPUTATIONALLY EFFICIENT ALGORITHMS FOR BROWNIAN DYNAMICS SIMULATION OF LONG FLEXIBLE MACROMOLECULES MODELED AS BEAD-ROD CHAINS

Mahdy Malekzadeh Moghani[1, a)] and Bamin Khomami[1, b)]
Materials Research and Innovation Laboratory, Department of Chemical and Biomolecular Engineering, University of Tennessee, Knoxville, Tennessee 37996, USA

(ΩDated: 10 January 2017)

The computational efficiency of Brownian Dynamics (BD) simulation of the constrained model of a polymeric chain (bead-rod) with n beads and in presence of hydrodynamic interaction (HI) is reduced to the order of n^2 via a novel algorithm which utilizes the conjugate-gradient (CG) method within a Picard iteration scheme. Moreover, the utility of the Barnes and Hut (B&H) multipole method in BD simulation of polymeric solutions in presence of HI, with regard to computational cost, scaling and accuracy, is discussed. Overall, it is determined that this approach leads to a scaling of $O(n^{1.2})$. Furthermore, a novel stress algorithm is developed which accurately captures the transient stress growth in the start-up of flow for the bead-rod model with HI and excluded volume interaction (EV). Rheological properties of the chains up to $n = 350$ in the presence of EV and HI are computed, via the former algorithm. The result depicts qualitative differences in shear thinning behavior of the polymeric solutions in the intermediate values of the Weissenburg number ($10 < Wi < 300$) when compared to ideal chains with HI. Moreover, the reduction of root mean square end to end distance, r_e, at high Wi under shear flow is shown to be the consequence of frozen folded state in the third (neutral) direction for systems with HI and EV. The uniaxial extensional flow of polymeric solutions has also been investigated and it's shown that the critical strain rates scales with $n^{1.6}$ which is also commensurate with the scaling of the longest relaxation time for systems with HI and EV.

I. INTRODUCTION

Molecular models with constraints are the backbone of various computational efforts aimed at investigating the dynamics of individual or assembly of macromolecules, therefore any improvement in this class of simulation techniques will not only enable more accurate and efficient simulation of macromolecules but also will positively impact closely related problems with holonomic constraints in classical molecular dynamic,[1,2] quantum chemistry[3] and econophysics.[4,5] Since consideration of macromolecules as a chain of uncorrelated segments by Kuhn, several constrained models of polymeric chain such as the freely jointed and the freely rotating chains have been introduced. These models have successfully predicted equilibrium and near-equilibrium properties of macromolecules via retarded motion expansion and variational methods. These findings have in turn facilitated development of coarse-grained micromechanical models such as the bead-spring chains as well as continuum level constitutive equations.[6]

While theoretical treatment of dynamics of constrained macromolecular models is mainly performed in generalized coordinates, the result is limited to a few rigid segments ($n < 4$) or small Peclet numbers($Pe = \dot{\gamma}\zeta l^2/kT$ where $\dot{\gamma}$ is the shear rate, ζ is the friction factor and l is the bead-bead bond length).[7–9] Development of robust integration techniques[10] for stochastic differential equations along with the steady improvement of computational resources have enabled dynamic simulation of constrained models of longer, or equivalently more flexible, chains with HI and EV via BD simulation. Meanwhile, single molecule techniques have provided tools to investigate and perturb semi-flexible chain,[11] and recently flexible chain[12,13], at the molecular level, which further motivates development of efficient computational methods. Specifically, BD algorithms need to go beyond modeling of approximately 150-200 statistical segments suitable for semi-flexible chains (e.g. λ-DNA), into algorithms that are capable of modeling 1000 or more Kuhn steps in order to examine dynamics of flexible polymers such as single stranded DNA.

Temporal evolution of segmental position of bead-spring chains can be performed via the well-known sweeping or semi-implicit algorithms; however, in the bead-rod model, in order to impose the constraint equations, a set of Lagrangian multipliers must be found via solution of a non-linear set of equations. For free draining (FD) chains, i.e., no HI, this is typically done by the well known Picard or Newton-Raphson algorithms,[14] via formation of a tri-diagonal coefficient matrix. Since the computational cost scales with $O(n)$, for n beads, the only obstacle to simulate chains with large n is the longest relaxation time of the chain which scales with $O(n^{\approx 2})$ and this translate to $O(n^3)$ scaling in computational cost as degree of polymerization increases. Proper implementation of various parallelization platforms allows simulation of $O(10^3)$ beads,[15] within reasonable computational time. However, in the presence of HI the aforementioned coef-

[a)] Current address: Goodyear Innovation Center, The Goodyear Tire and Rubber Company, Akron, Ohio 44316, USA
[b)] Electronic mail: bkhomami@utk.edu

ficient matrix is dense, and in order to take advantage of the multipole or CG methods, it has to be rewritten as an operation between a set of known vectors rather than matrix-vector products. This immediately rules out use of any second order method such as the Newton-Raphson method. This problem can be eliminated by including an iterative CG method based on the Krylov subspace within a Picard algorithm. As shown below, this combination significantly improves the performance of BD simulation of the bead-rod model with HI and reduces the scaling exponent from 3 to 2.

Also in presence of HI, the inherent $O(n^3)$ cost of commonly used Cholesky decomposition technique to find the correct weighting matrix of the random forces (also known as the correlation tensor) from the diffusion tensor is the major obstacle to reduce the scaling exponent of computational cost of the BD simulation. To this end, several techniques such as the Chebyshev polynomial expansion have been introduced, in order to effectively reduce the computational cost to $O(n^{2.25})$ for long chains[16–18]. More importantly, fast multipole methods (FMM) have recently been developed by Liang *et al.*[19] that allow $O(n \log n)$ scaling.

In this study, we have utilized the Barnes and Hut (B&H) method[20] that also gives rise to $O(n \log n)$ for the formation of the mobility matrix. It should also be noted that the B&H method is preferred to the FMM in this case since it can be modified to ensure fulfillment of Newton's third law of motion,[21] which ensures accurate scaling of diffusion and other dynamic properties. Furthermore, in our method the correlation tensor is constructed via the Krylov subspace method to reduce the computational cost for inclusion of HI.[18,22]

Overall, in this study we have developed three main algorithms in presence of HI and EV: 1)a combined Picard-Conjugate Gradient (CG) method with $O(n^2)$ scaling 2)an implementation of the B&H multipole method within the Picard-CG iteration technique to yield a scaling of $O(n^{1.25})$ and 3)a stress calculation algorithm that allows accurate computation of polymer contribution to the stress tensor at steady state but more importantly, under transient conditions. Specifically, the polymeric stress is decomposed into contributions from each force within the framework developed by Morse[23]. Further, the aforementioned techniques are utilized in order to examine the non-equilibrium behavior (diffusion, shear and extensional flow) of polymeric solutions in presence of HI and EV.

Petera and Muthukumar[24] have explored the steady state material functions of dilute polymeric solutions with the bead-rod model with inclusion of HI and EV for small chains ($n < 20$) under shear flow. Their results depict that HI has three effects on the shear properties of polymeric solution. First, the absolute value of shear thinning slope decreases. Second, the viscosity is lowered at small shear rates when compared to the FD chain with EV. Third, the first normal stress coefficient (ψ_1) is smaller than the FD chain at low shear rates and larger after a critical shear rate of $O(100)$ bead diffusion time. Utilizing the same bead-rod model, Liu, Ashok, and Muthukumar[25] studied macromolecular dynamics in elongation flow of a dilute polymeric solution and found that at the coil-stretch transition $\dot{e}_c \sim n^{-\alpha}$; for $n \leq 60$ and $\alpha = 1.4$. Their prediction is in good quantitative agreement with experimental measurements, i.e., 1.5, irrespective of the solvent quality. Neelov *et al.*[26] found the scaling exponent $\alpha = 1.55$ with HI ($n < 100$) and 1.96 for the FD case. Sim, Khomami, and Sureshkumar[27] employed the bead-rod model to investigate scission due to segmental tension ($n < 150$) and showed that $\dot{e}_c \sim n^{-2}$ with no HI and $\dot{e}_c \sim n^{-1.7}$ with HI and EV. This difference is contributed to the fact that HI effectively shields the inner beads from bulk flow and increases the time required for coil-stretch transition at $\dot{e}_c$.[28] It has also been shown[29] that translational diffusivity of the polymeric chain in dilute solution scales as $\sim n^{-0.579}$.This prediction is in good agreement with other simulation and the experimental observations, $D \sim {n_b}^{-0.55<\gamma<-0.68}$, as discussed in more details in the next section.

II. THEORY OF CONSTRAINED BROWNIAN MOTION

In this sections, first the aforementioned three new algorithms are introduced. Subsequently, in the result and discussion section, both shear thinning and coil stretch transition are discussed for chains of length $n = 100$ and $n = 350$ in presence of HI and EV.

A. Problem formulation

The contour length of the polymeric chain (l) is divided into n_s segments with fixed length (l_o), each representing the equilibrium Kuhn length of a free rotating chains with no intramolecular interactions. Mathematically, the fixed Kuhn length can be shown as a set of n_s constraints: $C(\{R\}) = |R_{\nu,\nu+1}|-1 = 0$ where $R_{\mu,\nu} \equiv R_\mu - R_\nu$ and R_i is the position vector of bead i. The phase-space trajectory evolution of $2n_s - 1$ degrees of freedom of such chain can be expressed via a stochastic differential equation subject to a set of constraints for the Kuhn length:

$$\Delta R/dt = \mathrm{P}\cdot(V^s + \kappa \cdot R + \mathrm{Y}\cdot F) + kT\frac{\partial}{\partial R}\cdot(\mathrm{P}\cdot\mathrm{Y}\cdot\mathrm{P}) \quad (1)$$

where P is the dynamical projection tensor and Y is the Rotne-Prager-Yamakawa (RPY) mobility tensor. R is the vector of $3n_b$ bead positions subjected to the solvent flow field with the velocity gradient (3×3 block diagonal) tensor of rank $3n_s$, $\bar{\bar{\kappa}}$, and uniform velocity V^s at the bead center. Vector F in Eq. 1 is the sum of the random force, metric force and the conservative force resulting from the inter-bead potential.

The random force is constructed as $F^{(r)} = \sqrt{2kT/dt}\zeta\cdot \mathrm{B}\cdot W$, where ζ is the Cartesian friction tensor, W is the vector of random numbers with variance of one and

mean of zero, and B is found via the Krylov subspace method[18] such that Y=B · B. The metric force is defined as $F^{(m)} = \frac{kT}{2}\frac{\partial}{\partial R}\ln[\det(\hat{\mathrm{G}})]$, where $\hat{\mathrm{G}} = \frac{1}{m}\mathrm{N}\cdot\mathrm{N}^{\dagger}$ and $\mathrm{N}^{i}_{\mu} = \frac{\partial c^{i}}{\partial R^{\mu}}$ is the vector normal to the constraint surface. Calculation of the metric force is facilitated using the following identity: $F^{(m)} = \frac{kT}{2}\frac{\partial}{\partial R}\ln[\det(\hat{\mathrm{G}})] = \frac{kT}{2}\hat{\mathrm{G}}^{-1}{:}\frac{\partial\hat{\mathrm{G}}}{\partial R}$ which allows utilization of the bidiagonal nature of N (See Appendix C). Finally, the inter-bead potential is limited to the hard sphere potential, hence the conservative force is given by $F^{(hs)} = \frac{\partial}{\partial R}\Phi(|R_{\nu\mu}|)$ where $\Phi(r) = 4\epsilon\left[\left(\frac{\sigma}{r}\right)^{12} - \left(\frac{\sigma}{r}\right)^{6}\right]$ for $r < 2^{(1/6)}\sigma = a$ and zero otherwise. In this study, the value of $a = 0.9$ and $\epsilon = \sqrt{dt}$ since this combination is shown to capture the correct force-extension curve[15]. In the following discussion, equations are nondimensoinalized as follows: l_o serves as the characteristic length scale, the characteristic time scale is the bead diffusion time $\zeta {l_o}^2/k_BT$ and forces are made dimensionless with k_BT/l_o.

B. Numerical algorithm

In formulating the numerical algorithm, we take advantage of the fact that it is not necessary to form the projection matrix in Eq.1 explicitly; instead, a two step algorithm with an Ito unconstrained move followed by a Stratonovich corrector step will reproduce the SDE in Eq.1. The Predictor step evolves the bead position vector $(R(t))$ to $\tilde{R}$, with the velocity equal to that of the terms inside the parenthesis in the first term of the right hand side of Eq.1, with all the chain configuration dependent terms calculated at time t. As noted earlier, the CPU intensive part of the algorithm for evolution of bead positions is associated with determination of the Lagrange multipliers from the following set of non-linear coupled equations (for $0 < \mu < n$):

$$\left[R^{*}_{\mu+1} + Y_{\mu+1}\cdot F^{(c)}\delta t - R^{*}_{\mu} - Y_{\mu}\cdot F^{(c)}\delta t\right]^{2} = 1 \quad (2)$$

Both Y and N terms are calculated at $R^{*} = (R(t) + \tilde{R})/2$, so that $R(t+dt) = \tilde{R} + \mathrm{Y}\cdot\mathrm{N}\cdot\Lambda = \tilde{R} + F^{(c)}dt$, where Λ is the vector of the n_s Lagrange multipliers, and in the right hand side expression $F^{(c)}$ is the constraint force. The new numerical iteration scheme reduces the computational cost of this step to the order of calculation of the RPY kernel (see Eq.4) on the force vector, instead of the typical $O(n^3)$ scaling required to solve the dense n_s non-linear system of equation that arises from the enforcement of the constraints in the corrector step. While utilizing the straight forward diffusion matrix formation and performing the $\mathrm{Y}\cdot F$ matrix-vector multiplication which results in an $O(n_s^{\approx 2})$ algorithm, the flexibility of the aforementioned numerical algorithm allows for incorporation of multipole methods. Specifically, the B&H tree method can be exploited as described in the next section in an attempt to attain the $n\log(n)$ theoretical scaling.

The coupled system of equations to determine the Λ vector for the segment i is found from the following equation:

$$\begin{aligned}&2\Big(\tilde{\mathrm{U}}\cdot\mathrm{S}\cdot\mathrm{Y}\cdot\mathrm{S}^{\dagger}\cdot\mathrm{U}\cdot\Lambda\Big)_{i,i}\\ &= 1 - \Big(\mathrm{S}\cdot\mathrm{Y}\cdot\mathrm{S}^{\dagger}\cdot\mathrm{U}\cdot\Lambda\Big)_{i,i}\Big(\mathrm{S}\cdot\mathrm{Y}\cdot\mathrm{S}^{\dagger}\cdot\mathrm{U}\cdot\Lambda\Big)_{i,i} - \tilde{U}_{i,i}\tilde{U}_{i,i}\end{aligned} \quad (3)$$

Both U and $\tilde{\mathrm{U}}$ are $3n\times n_s$ and S, the Grand Rouse matrix, is $3n_s \times 3n_b$.

The solution algorithm is summarized in algorithm 1 of the supplemental material section I. The next step of the corrector step, involves utilization of the CG method for solving the linear system $\left(\tilde{\mathrm{U}}\cdot\mathrm{S}\cdot\mathrm{Y}\cdot\mathrm{S}^{\dagger}\cdot\mathrm{U}\right)$ (see algorithm 2 in the supplemental material section I). In both steps, the matrix-vector kernel can be performed by a suitable routine, i.e., direct or B&H method depending on the system size as discussed in the next section.

C. Application of the B&H method in constrained BD

The 3×3 blocks of the RPY HI tensor of the bead-rod model of a macromolecule, nondimensionalized with kT/ζ, can be written as:

$$\Omega_{ij} = \quad (4)$$
$$\begin{cases} \frac{3a}{4|R_{ij}|}\left[\left(1+\frac{2a^2}{3|R_{ij}|^2}\right)\iota + \left(1-\frac{2a^2}{|R_{ij}|^2}\right)\frac{R_{ij}R_{ij}}{|R_{ij}|^2}\right] & |R_{ij}|\geq 2a \\ \left[\left(1-\frac{9|R_{ij}|}{32a}\right)\iota + \left(\frac{3}{32a|R_{ij}|}\right)R_{ij}R_{ij}\right] & |R_{ij}|< 2a \end{cases}$$

where a is the hydrodynamic radius which is set to 0.9 for all chains with HI in this study. The matrix-vector kernel is then:

$$V = \Omega\cdot F,$$

where V is the perturbation velocity due to HI, Ω is the hydrodynamic tensor and F is the force vector on the particles that creates the velocity perturbation (source particles). The aforementioned equations can be rewritten for the RPY matrix at distances greater than the bead diameter ($\alpha \in \{x,y,z\}$ and $\mathrm{r}_{ij} \equiv |R_{ij}|$):

$$\begin{aligned}V_{\alpha,i} = &\sum_{j\neq i}\left(c_1\frac{1}{\mathrm{r}_{ij}}F_{j,\alpha} + c_2\frac{1}{\mathrm{r}^3_{ij}}F_{j,\alpha}\right)\\ &+\sum_{j\neq i}\left(c_1\frac{R_{ij\,,\alpha}\,(R_{ij}\cdot F_j)}{\mathrm{r}^3_{ij}} - c_2\frac{3R_{ij,\alpha}\,(R_{ij}\cdot F_j)}{\mathrm{r}^5_{ij}}\right),\end{aligned}$$

with $c_1 \equiv 3a/4$ and $c_2 \equiv a^3/2$. Substituting R_{ij} in the above equation:

$$\begin{aligned}V_{\alpha,i} = &\sum_{j\neq i}\left(c_1\frac{1}{\mathrm{r}_{ij}}F_{j,\alpha} + c_2\frac{1}{\mathrm{r}^3_{ij}}F_{j,\alpha}\right)\\ &+\sum_{j\neq i}\left(c_1\frac{(R_i-R_j)_\gamma R_{ij,\alpha}F_{j,\gamma}}{\mathrm{r}^3_{ij}} - c_2\frac{3(R_i-R_j)_\gamma R_{ij,\alpha}F_{j,\gamma}}{\mathrm{r}^5_{ij}}\right)\end{aligned}$$

The last two terms can be expanded to yield:

$$V_{\alpha,i} = c_1 \sum_{j\neq i} \frac{1}{\mathrm{r}_{ij}} F_{j,\alpha} + c_2 \sum_{j\neq i} \frac{1}{\mathrm{r}_{ij}^3} F_{j,\alpha}$$
$$-c_1 r_{i,\gamma} \sum_{j\neq i} \frac{d}{dr_\alpha}\left(\frac{F_{j,\gamma}}{\mathrm{r}_{ij}}\right) + c_2 r_{i,\gamma} \sum_{j\neq i} \frac{d}{dr_\alpha}\left(\frac{F_{j,\gamma}}{\mathrm{r}_{ij}^3}\right)$$
$$+c_1 \sum_{j\neq i} \frac{d}{dr_\alpha}\left(\frac{r_{j,\gamma}F_{j,\gamma}}{\mathrm{r}_{ij}}\right) - c_2 \sum_{j\neq i} \frac{d}{dr_\alpha}\left(\frac{r_{j,\gamma}F_{j,\gamma}}{\mathrm{r}_{ij}^3}\right) \quad (5)$$

$$V_{\alpha,i} = c_1\phi_{1/r,\alpha,i} + c_2\phi_{1/r^3,\alpha,i} - c_1\psi_{1/r,\alpha,i} + c_2\psi_{1/r^3,\alpha,i} + c_1\chi_{1/r,\alpha,i} - c_2\chi_{1/r^3,\alpha,i} \quad (6)$$

Eq. 6 defines $\phi(F,R)$, $\psi(F,R)$ and $\chi(F,R)$. Both ϕ and ψ can be constructed from the same multipole moments and sources, therefore significantly reducing the associated computational overhead as demonstrated below. The χ terms also share the same multipole moments, i.e., $r_{j,\gamma}F_{j,\gamma}$, so they are efficiently merged into a common tree formation (built up) and force calculation routine.

Consider the above potential at $R_{ij} = R_i - R_j = R_i - R_{c,m} + (R_{c,m} - R_j)$, where $R_{c,m}$ is center of force of m particles:

$$R_{ij} = R_{i,c} + \delta R_{c,m}$$

$$R = R_{i,c} \equiv R_i - R_{c,m}$$

$$\delta R = \delta R_{c,j} \equiv (R_{c,m} - R_j)$$

Note that R is only a function of the jth particle position and not each individual source particle; hence it can be factored out of the sum. A Taylor expansion of the kernel,

$$f_{\alpha,i}(R+\delta R) = \sum_j^N \Big[f_{\alpha,i}(R) + \frac{\partial f_{\alpha,i}(r_i)}{\partial r_i}|_R \cdot \delta R_{c,j} + \frac{1}{2}\delta R \cdot \frac{\partial^2 f_{\alpha,i}(r_i)}{\partial r_i \partial r_i}|_R \cdot \delta R_{c,j} \Big]$$

allows each term on the RHS of Eq. 6 to be determined (see Appendix B).

1. B&H method in BD: summary of implementation

The classical implementation of the B&H method starts by hierarchical division of the simulation box (tree) into sub-spaces (tree branches) until every source point is assigned to one and only one sub-space (leaf). In 2-dimension for instance, the first division of the two dimensional box-square leads to four squares with sides half the size of the original square (quad-trees), in turn each is divided into 4 smaller squares. Each branch has a center of force and the center of force of the leaves are indeed the position vector of the beads. Under certain condition, namely, the θ condition is met (see below for details), the HI between the cluster of beads in a sub-space will not sum over every individual particle in the sub-space, but it is estimated indirectly through the multipole components of that specific box. The aforementioned condition is determined by a preset value of θ: for each particle i and box with center of force r_{cm} and the length of the box edge, l_{box}, if $\theta < \frac{l_{box}}{r_{i,cm}}$ then the multipole effects are considered, otherwise one should move one level down the tree and consider the branches (children) of the original box. In the case of HI in BD simulation, consideration of the following four essential conditions in the code results in significant enhancement of the computational efficiency. First, in the corrector step bead positions are not changed, hence, in the subsequent Picard iterations it is not required to update the tree. Second, considering the number of CPU operations required to estimate the RHS of Eq. 6 for any branch with less than 3 beads, HI is calculated directly from each bead. Third, the direct interactions amongst all bead pairs can be summarized in the grand sparse mobility tensor of rank $3n$, which is also unchanged during the corrector step. Finally, the indirect multipole interactions are also summarized in a tensorial format, which should be recalculated in each iteration. This last step, is the most time consuming step of the B&H method for implementation of HI in the bead-rod BD simulations; future efforts should especially target enhancing the efficiency of this step.

D. Stress calculation

While formulation of stress tensor in terms of force vector and conformation tensor is readily available for dilute polymeric solution models both with and without HI[6,10,30]; the existing algorithms for estimation of the transient stress tensor for dilute polymeric systems described with micromechanical models with constrains is limited to the case with no HI.[27] Although the existing algorithms discuss the various methods for noise reduction either via Stratonovich method, with separation of Brownian and viscous contribution,[31] or Ito formulation,[32] there are no established algorithm that allows accurate determination of the transient stress for the bead-rod description of dilute polymeric solution in presence of HI due to the relatively large error associated with the stochastic force, especially at small $Wi = Pe\lambda_\Delta$.[27]A summary of stress algorithms can be found in the excellent review by Morse.[23] Our proposed algorithm decomposes the stress into deterministic and stochastic portions using the projection matrix; this also allows determination of the contribution of each deterministic force such as the metric force or potentials individually. Hence, in the transient regime, due to this novel noise reduction technique, this method produces accurate results with limited number of trajectories.

1. Stress calculation: summary of implementation

In order to find the noise reduced stress, it is necessary to decompose the tensions (constraint forces, i.e., $F^{(c)}$) into a stochastic and deterministic part. In the Öttinger[30] algorithm the total drift velocity in terms of all forces is determined as:

$$dR/dt = \Upsilon \cdot \left(F^{(r)} + F^{(f)} + F^{(\phi)} + F^{(e)}\right) + \tilde{\Upsilon} \cdot \tilde{\mathrm{N}} \cdot \Lambda \quad (7)$$

, where $\mathrm{N} \equiv \nabla_r \mathrm{C}$.

The total drift velocity must occur adjacent to the hyper surface defined by the constraints:

$$\mathrm{N} \cdot \Delta R = 0$$
$$= \mathrm{N} \cdot \left[\Upsilon \cdot \left(F^{(r)} + F^{(f)} + F^{(\phi)} + F^{(e)}\right) + \Upsilon^* \cdot \mathrm{N}^{*\dagger} \cdot \Lambda\right]$$

For a linear chain this condition clearly can be rewritten as $-2U_i \cdot dR_{i-1} + 2U_i.dR_i = 0$ with $U_i = R_i - R_{i-1}$. This in turn can be rewritten as $2U_i \cdot dU_i = dU_i^2 = 0$ or constant bond length if N is calculated at the end of each time step. The tension values then will be given by:

$$\left[\mathrm{N} \cdot \Upsilon^* \cdot \mathrm{N}^{*\dagger}\right]^{-1} \cdot \mathrm{N} \cdot \Upsilon \cdot \left(F^{(r)} + F^{(f)} + F^{(\phi)} + F^{(e)}\right) = \Lambda$$
$$= \Lambda^{(r)} + \Lambda^{(f)} + \Lambda^{(\phi)} + \Lambda^{(e)}$$

Each tension term on the RHS is defined corresponding to the decomposition of total force on the LHS, respectively. The stochastic and deterministic portion of the constraint forces are then easily defined via the following expressions, $F^{(c,r)} = n^{*\dagger} \cdot \Lambda^{(r)}$ and $F^{(c,d)} = n^{*\dagger} \cdot \left(\Lambda^{(f)} + \Lambda^{(\phi)} + \Lambda^{(e)}\right)$. The deterministic drift velocity due to each of the forces is simply found from: $\Upsilon \cdot F$. For the RPY HI tensor with no external forces, the polymer contribution to the stress tensor can be found from:

$$\bar{\bar{\tau}} = \sum R_\mu \tilde{\zeta} \cdot (\tilde{V}_\mu - V^s - \kappa \cdot R) + kT\,(tr(\mathrm{P}) - \iota) \quad (8)$$

where $\tilde{\zeta}$ is the modified effective friction tensor as defined in equation (5.4) of Öttinger[30] and $\mathrm{P} = \mathrm{I}\text{-}\left[\mathrm{N} \cdot \Upsilon^* \cdot \mathrm{N}^{*\dagger}\right]^{-1} \cdot \Upsilon^*$ is the projection tensor corresponding to the numerical midpoint algorithm.

III. RESULT AND DISCUSSION

To determine the relative computational efficiency of each algorithm as function of the number of beads in a given chain in a dilute solution, the relative performance, computational cost and accuracy of the B&H method versus the direct formation of the mobility tensor is discussed first. In turn, the efficiency of the estimation of the correlation tensor of the stochastic force via the Krylov subspace method and the Cholesky decomposition of the mobility tensor is considered.

The computational efficiency of the proposed Picard-CG in the corrector step , in which the constraint forces are calculated, is compared with the naïve matrix inversion known to require $O(n^3)$ operations.

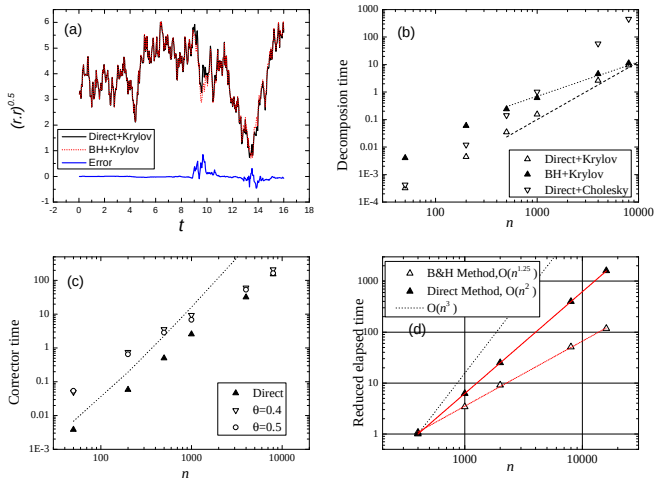

FIG. 1. (a) Simulation of a single chain trajectory at equilibrium. (b) The relative performance of algorithms in terms of wall clock time (sec.) per one step. (c) The corrector computational time and the scaling factor in the B&H method are both reduced by increasing the θ criterion from 0.4 to 0.5. Terms until the first dipole are considered in obtaining the above results. (d) The scaling of the computational cost of each method. Elapsed time is normalized by the time required by *each* method for n=400.

A. Accuracy and performance of the B&H method

In order to determine the accuracy of the B&H method, a single chain trajectory obtained via this method is compared with the trajectory obtained from the direct formation of the RPY HI tensor. As shown in Fig. 1-a; the two trajectories almost exactly follow the same path and there is no error accumulation for a chain with 25 beads. Moreover, the random error falls within a few percentage of the observable value. Comparison of the decomposition times, for a wide range of n, reveals that the direct formation of mobility tensor with Krylov subspace method is the most efficient method for a wide range of practical chain sizes, while the B&H method becomes the more efficient method at about $n^* \approx 12000$ (n^* is the number of beads in the system at which the B&H method outpaces the direct Krylov method). The corrector step CPU time shows a similar trend (see Fig. 1-c); As expected, the parameter θ , which determines the threshold of substitution of the multipole effect of the source instead of the direct effect, reduces n^*. The theoretical computational cost of the code using the naïve method (Cholesky decomposition) is $O(n^3)$ for large n, however the scaling exponent of the elapsed time vs. the number of beads is about 1.25 for the B&H method, compared to the value of 2 for the direct method utilizing the Krylov subspace technique. Both B&H and direct method are implemented in the Picard-CG algorithm.

Three important factor should be considered in interpreting the aforementioned results. First, the bottleneck of calculation within both decomposition and cor-

rector steps is the matrix-vector multiplication. In case of the direct method, all multiplications are performed via the highly optimized Intel MKL library, while the B&H method relies on the inferior optimization offered by the authors. The B&H implementation should be around 4 times faster than its current version in order to surpass the Direct-Krylov method for a chain of $n = 1000$. It is highly likely that a tailor-made code targeted for an optimized B&H method could further reduce the n^* value. Next, the timings reported here are estimated from a single chain at equilibrium. The equilibrium condition in which the chain bead-to-bead distance distribution follows the Gaussian distribution constitutes an unfavorable condition for the B&H method compared to a uniform distribution or a stretched chain under flow. Moreover, in the semi-dilute regime where several chains are present in the simulation box, the B&H method gains a significant advantage. Specifically, in the semi-dilute regime, where distances between chains center of mass are relatively long, i.e., existence of favorable θ values, the multipole effect of the neighboring chain replaces the many contributions from individual bead-bead interactions.

The long-time limit ($t > \lambda$) of the translational diffusion coefficient of the center of mass of the chain (D) follows theoretically determined power law scaling with the size of the chain. For the free-draining Gaussian chain $D \sim n^{-1.0}$, while for a Zimm model, HI enhances the diffusion so that $D \sim n^{-3/5}$. The corresponding value from the simulation:

$$D \sim \frac{1}{nt}\lim_{t\to\infty}\left(\left\langle\sum r_{ij}(t)\right\rangle - \left\langle\sum r_{ij}(0)\right\rangle\right)$$

of each chain type, is shown in Fig.2. The ideal (no EV) and real (with EV) free-draining chains scaling agrees well with the theoretical predictions of the Rouse model. For the chain with HI, both in Θ- and good-solvent, the scaling exponent is in good agreement with theory and experiment.[33]

The longest relaxation time of the polymer chain was found via Birefringence value as described by Doyle, Shaqfeh, and Gast.[31] Similar values obtained via an exponential fit to the last 10% of the conformational relaxation of the fully-extended chains are also shown in Table I; however, in order to rescale the Pe to Wi, the former values where utilized ($\lambda = \lambda_\Delta$). Closer examination of the relaxation plot of r_e reveals two regimes of relaxation spectrum: at high extension ($x = (r \cdot r)^{0.5}/n > 0.6$) the relaxation is influenced by HI; therefore, irrespective of the EV interactions, chains with HI demonstrate similar relaxation behavior. On the other hand, below $x = 0.5$, (see Fig.3) the EV interaction dominates the relaxation behavior, consequently, the relaxation process slows down and the scaling exponent of the longest relaxation time with the molecular weight increases from 2.0 (for ideal FD chain) to 2.2 (for chains with EV but no HI). Moreover, as seen in Fig. 3, the pairs with the EV , i.e., real free draining and with HI in good-solvent, follow a similar slope, while the (ideal free draining and

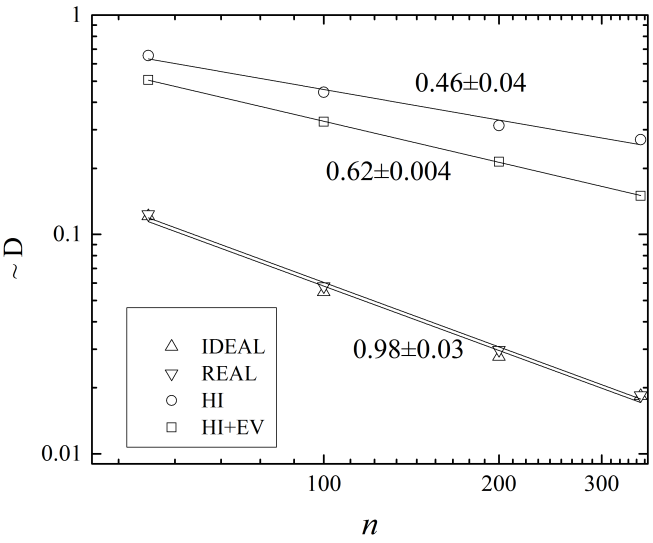

FIG. 2. Scaling of the translational diffusion coefficient of the chain center of mass. HI significantly increases the diffusion coefficient and EV effect on the scaling is only significant in presence of HI.

TABLE I. Longest relaxation time of bead rod chains obtained via birefringence and r_e relaxation of fully extended chains from BD simulation.

	Ideal FD		Real FD		HI Θ-solvent		HI Good-solvent	
n	Δ	r_e	Δ	r_e	Δ	r_e	Δ	r_e
49	43	38	56	61	15	22	19	32
99	162	198	266	362	43.8	66	60	114
199	595	904	1145	1569	119	197	172	265
349	1783	2600	3984	5410	230	-	420	-

with HI in a Θ-solvent) curves are parallel to each other. This leads to the conclusion that below $x = 0.5$ the relaxation process is greatly influenced by EV effects. It should be noted that the extension at which the transition between these two regimes occurs is roughly equal to the extension at which the Langevin and the force law for real chains intercept.[15]

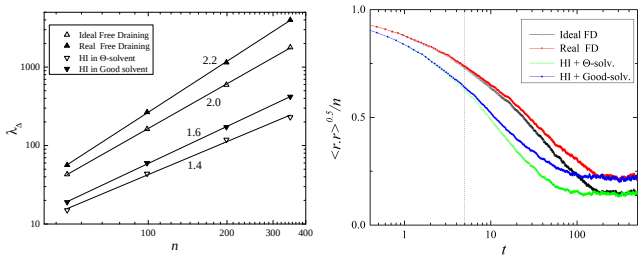

FIG. 3. Scaling of the longest relaxation time (left). Relaxation plot of the end-to-end distance (right). The dotted line qualitatively separates the two regions.

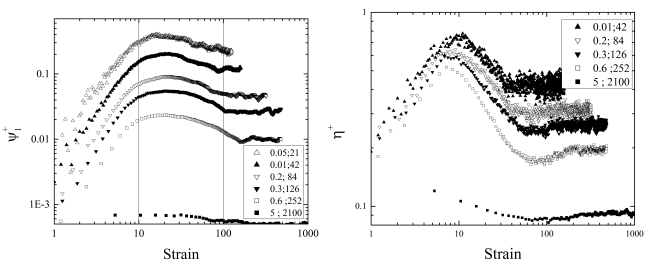

FIG. 4. Transient rheological properties of the chain with HI in a good solvent ($n = 350$) for the start-up of a shear flow. The legend is the $(Pe; Wi)$ pair.

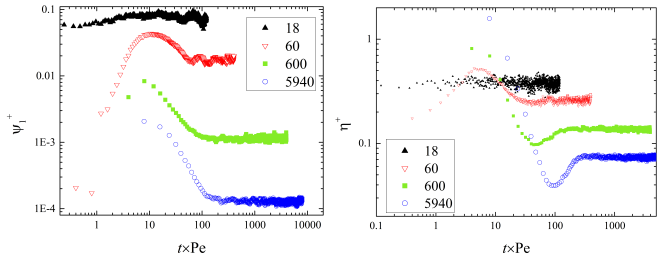

FIG. 5. Transient rheological properties of chain with HI in a good solvent ($n = 100$) subjected to start-up of shear flow. The Wi for each data set is shown in the legend.

B. Shear flow: transient and steady state properties

In order to test the proposed stress estimation algorithm, the rheological properties of macromolecules in a good solvent in presence of HI are examined. The contribution of the polymer chain to the stress tensor is calculated for both shear flow and uniaxial extension flow kinematics over a broad range of Wi for chains with $n = 100$ and $n = 350$. The ensemble size is set to 256 chains (due to parallel implementation, size of the ensemble does not affect the simulation time). The latter chain is at least twice the size of the largest chain considered in the literature; hence, the results should provide a better estimate of the effect of EV, i.e., closer to the long chain limit also referred to as universal behavior.[15]

The transient viscosity (η^+) and first normal stress coefficient (ψ^+) for start-up of shear flow are shown in Fig. 4 and Fig. 5 for an ensemble of 256 chains. The overshoot of first normal stress coefficient, for $Wi > 10$, occurs at about 10-30 strain units (Fig. 4a and Fig. 5a). The magnitude of the overshoot $\psi^+_{max} \sim Wi^{-0.635}$. In the case of transient viscosity, the maximum occurs at slightly smaller Henky strain, and more importantly, at large Wi it is followed by a minima before it plateaus at the steady state level. Although the maxima is well characterized by the Henky strain and it is in exact agreement with experimental observation of start-up of DNA solutions,[34] the minima in the shear viscosity shifts to higher Henky stresses as Wi increases. The magnitude of the maximum shear viscosity contribution of the polymer in the range shown in Fig. 4b follows $\eta^+_{max} \sim Wi^{0.266}$. For ideal free draining chain this exponent is 0.4-0.45. The overshoot and oscillatory behavior of the shear stress components also appears in the conformational relaxation of the polymeric chain[35]. However as shown in Fig. 6a, the overshoot in r_e as a measure of chain conformation is out of phase when compared to the overshoot of the stress, which consistently occurs around 10-30 strain units ($10 < \gamma_{max} < 30$). This phase shift between conformation and stress results in an oscillatory behavior that extends beyond the longest relaxation time, and the frequency of the oscillation increases with Wi as shown in Fig. 6b.

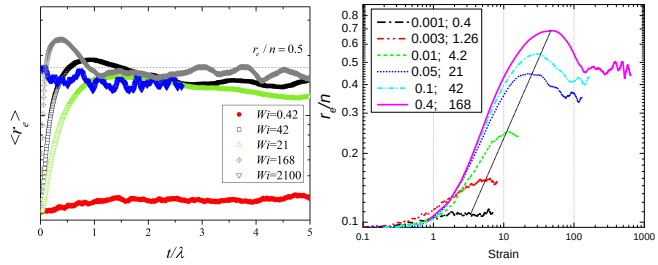

FIG. 6. Transient conformational properties of chain with HI in a good-solvent ($n = 350$) for start-up of shear flow. The Wi for each data set is shown in the legend. The left figure illustrates the oscillatory behavior which continues over couple of relaxation times and on the right, wide variations of the strain at the overshoot γ_{max} with flow strength is depicted.

EV and HI also affect the shear-thinning behavior of the rheological properties. In general, our results indicate that the shear-thinning behavior for both shear viscosity (η) and first normal stress coefficient (ψ_1) at high Wi is close to the estimates of Doyle, Shaqfeh, and Gast[31], i.e., $\psi \sim Wi^{-14/11}$). However in the intermediate Wi the absolute value of the power law exponent is smaller, and the exponent is not fixed at $-4/3$ ($\psi \sim Wi^{-4/3}$), irrespective of HI and EV as it was concluded earlier for $n < 150$.[36] In the case of shear viscosity, Petera and Muthukumar[24] attained a power-law exponent of approximately -0.5 ($\eta \sim Wi^{-0.5}$) in the presence of HI and EV for shorter chains ($n < 20$), which is similar to the exponent of free-draining chain,[31,37] while Hur, Shaqfeh, and Larson[38] found a scaling of -0.257 from bead-spring simulations.[39] Fig. 7 demonstrates the shear thinning properties of dilute solution of polymers in a good solvent calculated in this work for both $n = 100$ and $n = 350$. As expected, both chains demonstrate power-low behavior. For $n = 100$ a single exponent of -0.28 fits the region of $10 < Wi$ while for the longer chain ($n = 350$), the shear thinning exponents is -0.4315 in the region $30 < Wi < 1000$ and the -0.28 exponent is only found for $1000 < Wi$. In the case of $n = 350$ the pronounced non-linear region in the log-log plot $0.8 < Wi < 4$ corresponds to the non-linear F-X regime of the initial lin-

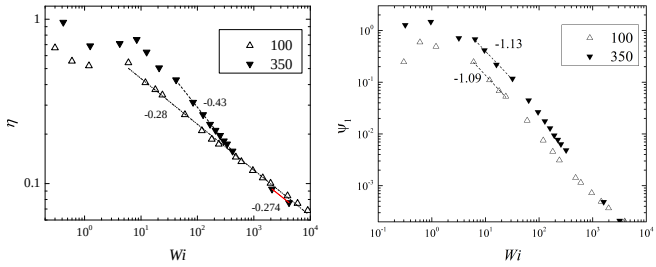

(a) Shear viscosity (b) First normal stress coefficient

FIG. 7. Steady-state scaling of shear rheology for a dilute solution of chains in a good solvent with HI. After the initial low shear rate plateau, longer chain show at last two regimes of shear thinning as discussed in the text.

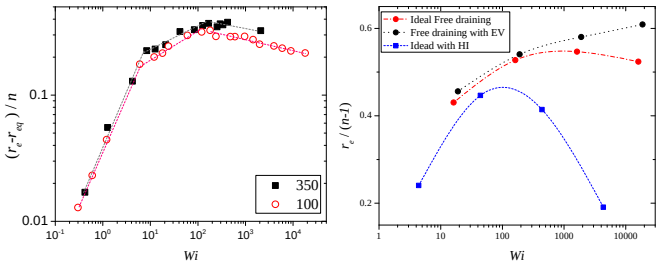

FIG. 8. Variation of the root mean squared end-to-end distance with Wi in shear flow. The plot on left demonstrates three distinct regimes of $r_e(Wi) - r_e(0)$. On the right, r_e is shown for ideal and real free draining chain and also chain only with HI and no EV interaction.

ear extension of polymeric chain. This initial regime for small Wi also appears in the scaling of the first normal stress coefficient (ψ_1) with a smaller absolute power-law exponent. While in the first shear-thinning regime (as depicted in Fig. 7b) $\psi \sim Wi^{-1.13}$, in the second regime $\psi \sim Wi^{-1.4}$. Although a similar trend exists for $n = 100$, the difference between two exponents is smaller (-1.09 and -1.14 for the second regime), these results are consistent with the smaller non-linear effects of EV for $n = 100$.[15]

Recent investigation of conformational properties of polymeric chain subject to HI and EV modeled as stiff Fraenkel springs have revealed a second region in the chain extension due to the shear flow in which the chain extension decreases as Wi increases.[40,41] This effect is captured in the bead-rod model presented in this research as well (Fig.8). It has been demonstrated that the shear plateau at $x \approx 0.5$ is due to the tumbling effect. Specifically, Dalal, Hoda, and Larson[41,42] have recently argued that reduced tumbling time (partial tumbling) of chain segments is the main mechanism that gives rise to chain shrinkage at very high Wi. However, the tumbling time for chains with no HI (free draining) scales similarly with Pe irrespective of EV despite the clear qualitative difference behavior of r_e variation at high Wi (See Fig. 8b). In order to describe this qualitative difference for chains without HI, it was argued that chains with EV are locked in a fully extended state.

An alternative explanation for the shrinkage observed in the aforementioned region is the existence of meta-stable folded conformations. The meta-stable folded conformations occur at high shear rates when a small portion of the chain that is folded on itself is frozen due to the strong aligning shear flow. For instance, in a chain with 100 segments *dynamic existence* of a small folded region with length 2 (total of 5 beads) can decrease r_e by 10%. Based on this hypothesis, an interaction that increases the possibility of such folds will result in a more pronounce shrinkage regime of r_e. In other words, the dynamic equilibrium between extended and folded state is shifted in favor of the folded states. For instance, HI as a overall cohesive potential will significantly enhance shrinkage of r_e as shown in Fig. 8b. In the absence of EV, HI results in chain conformation with beads that are unrealistically close together; the velocity of these two beads with small distance is strongly correlated due to the large coefficient of the HI tensor where other forces are relatively small. Hence, their translational degrees of freedom will be highly correlated. This results in a permanent folded region. On the other hand, repulsive potentials such as EV reduce the possibility of folded states and suppress the shrinkage of r_e. For chains with EV and no HI, formation of meta-stable folds is less likely since the strong velocity gradient in the second direction , i.e., direction of shear, will convect the beads away from each other. When both HI and EV are present, adjacent beads in a folded configuration can move into the neutral direction ($\vec{z}$) and create a fold in xz-plane. Detailed inspection of diagonal components of the radius of gyration reveals that when $r_{g,y} \to 1$ then $r_{g,z} \to 2$, this is equivalent to thickness of two beads, and stays constant as Wi increases (Fig. 9). Meanwhile, the τ_{zz} component of stress tensor increases, although the second normal stress coefficient stays close to zero, as demonstrated in Fig. 9c.

C. Uniaxial flow : coil-stretch transition

The uniaxial flow kinematics, such as the flow in filament stretching rheometer, include the interesting coil to stretch transition feature. Indeed, such effect is also observed in our BD flow simulations; as shown in Fig. 10a the coil-stretch transition approaches a first order transition as the number of segments increases. However, the critical Wi remains constant at ≈ 0.5. This suggests that the critical strain rate scales as $n^{1.6}$ for the chain in good solvent which is in good agreement with the experimental observation[27].

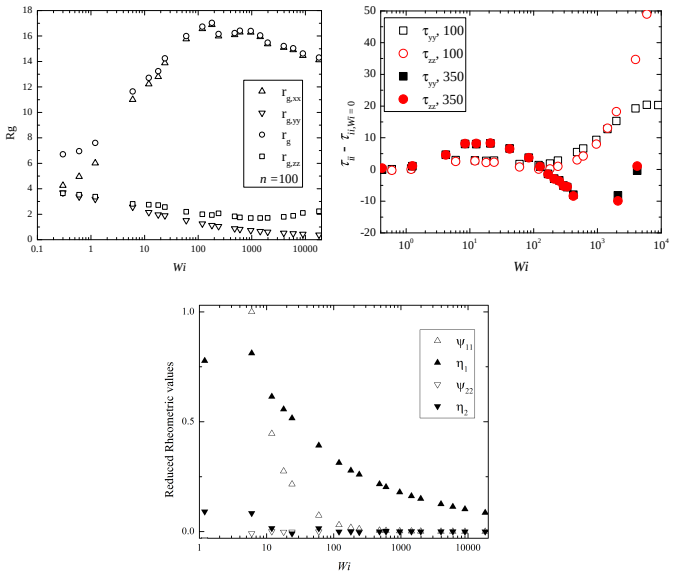

FIG. 9. Diagonal components of the (a) radius of gyration tensor and (b) the corresponding stress tensor components (chains with HI and EV). Despite the growth of diagonal components of the stress in velocity gradient and neutral direction, the second normal stress coefficient remains approximately zero (c).

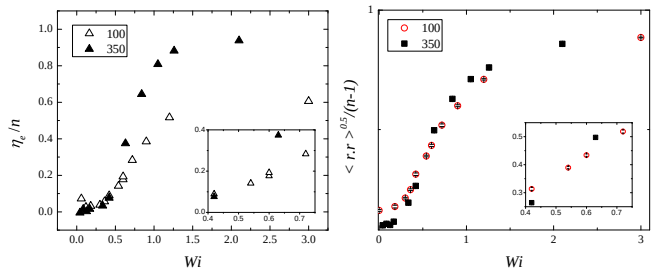

FIG. 10. The elongational viscosity (right) and coil to stretch transition for dilute polymeric solution subject to uniaxial flow kinematics

IV. SUMMARY

In summary, a new method for BD simulation of bead-rod model of dilute macromolecular solutions with HI is developed, which reduces the computational cost scaling to $n^{\approx 2}$. Incorporating the B&H based method reduces the scaling exponent of the computational cost further (to $n^{1.2}$). While the B&H method for dilute solutions at equilibrium is not superior to the Picard-CG direct method (except for $n > 10000$), its optimized application for the semi-dilute solutions should produce the theoretical $n \log(n)$ scaling and reduce the cross-over threshold to a smaller value of n.

Furthermore, a new algorithm for estimation of the stress tensor has been deployed to study transient rheological properties in shear and uniaxial flows. In the shear flow, consistent with the effect of EV on the force-extension curves,[15] at least two shear thinning regimes for shear rheological properties were observed. Moreover, close inspection of radius of gyration tensor and stress tensor components under shear flow and high Wi reveal existence of frozen states due to folds in the neutral (third) direction. It is also shown that the coil-stretch transition generated by uniaxial existential flow approaches a first order transition as n is increased and the critical strain rate scales with $n^{1.6}$.

ACKNOWLEDGMENTS

We would like to acknowledge the Sustainable Energy and Education Research Center at the University of Tennessee and the Department of Energy (DE-FG02-08ER46528) for financial support of this work. This research was also supported in part by an allocation of advanced computational resources on DARTER by the National Institute for Computational Sciences (NICS).

Appendix A: Picard+CG algorithm

Please see section I in supplemental material.

Appendix B: Computationally efficient multipole expansion of RPY

Please see section II in supplemental material.

Appendix C: The Metric force formulation

Please see section III in supplemental material.

[1] J.-P. Ryckaert, G. Ciccotti, and H. J. Berendsen, "Numerical integration of the cartesian equations of motion of a system with constraints: molecular dynamics of¡ i¿ n¡/i¿-alkanes," Journal of Computational Physics **23**, 327–341 (1977).
[2] S. Miyamoto and P. A. Kollman, "Settle: an analytical version of the shake and rattle algorithm for rigid water models," Journal of computational chemistry **13**, 952–962 (1992).
[3] P. Echenique, I. Calvo, and J. L. Alonso, "Quantum mechanical calculation of the effects of stiff and rigid constraints in the conformational equilibrium of the alanine dipeptide," Journal of Computational Chemistry **27**, 1733–1747 (2006).
[4] M. Schulz, *Statistical physics and economics: concepts, tools and applications*, Vol. 184 (Springer, 2003).
[5] J. Janovà, "Applications of a constrained mechanics methodology in economics," European Journal of Physics **32**, 1443 (2011).
[6] R. B. Bird, C. Curtiss, R. Armstrong, and O. Hassager, *Dynamics of Polymeric Liquids, 2 Volume Set* (Wiley-Interscience, 1996).
[7] H. A. Kramers, "The behavior of macromolecules in inhomogeneous flow," The Journal of Chemical Physics **14**, 415 (1946).
[8] J. G. Kirkwood and J. Riseman, "The intrinsic viscosities and diffusion constants of flexible macromolecules in solution," The Journal of Chemical Physics **16**, 565 (1948).

[9]O. Hassager, "Kinetic theory and rheology of bead-rod models for macromolecular solutions. i. equilibrium and steady flow properties," The Journal of Chemical Physics **60**, 2111–2124 (1974).

[10]H. C. Öttinger, "Brownian dynamics of rigid polymer chains with hydrodynamic interactions," Physical Review E **50**, 2696–2701 (1994).

[11]S. Smith, L. Finzi, and C. Bustamante, "Direct mechanical measurements of the elasticity of single dna molecules by using magnetic beads," Science **258**, 1122 (1992).

[12]O. A. Saleh, D. B. McIntosh, P. Pincus, and N. Ribeck, "Nonlinear low-force elasticity of single-stranded dna molecules," Physical Review Letters **102** (2009).

[13]A. B. Marciel and C. M. Schroeder, "New directions in single polymer dynamics," Journal of Polymer Science Part B: Polymer Physics **51**, 556–566 (2013).

[14]M. Somasi, B. Khomami, N. Woo, J. Hur, and E. Shaqfeh, "Brownian dynamics simulations of bead-rod and bead-spring chains: numerical algorithms and coarse-graining issues," Journal of Non-Newtonian Fluid Mechanics **108**, 227–255 (2002).

[15]M. M. Moghani and B. Khomami, "Flexible polyelectrolyte chain in a strong electrolyte solution: Insight into equilibrium properties and force-extension behavior from mesoscale simulation," The Journal of Chemical Physics **144**, 024903 (2016).

[16]R. Jendrejack, M. Graham, and J. De Pablo, "Hydrodynamic interactions in long chain polymers: Application of the chebyshev polynomial approximation in stochastic simulations," The Journal of Chemical Physics **113**, 2894 (2000).

[17]R. R. Schmidt, J. G. H. Cifre, and J. G. de la Torre, "Comparison of brownian dynamics algorithms with hydrodynamic interaction," The Journal of Chemical Physics **135**, 084116–10 (2011).

[18]T. Ando, E. Chow, Y. Saad, and J. Skolnick, "Krylov subspace methods for computing hydrodynamic interactions in brownian dynamics simulations," The Journal of Chemical Physics **137**, 064106–14 (2012).

[19]Z. Liang, Z. Gimbutas, L. Greengard, J. Huang, and S. Jiang, "A fast multipole method for the rotnepprageryamakawa tensor and its applications," Journal of Computational Physics **234**, 133–139 (2013).

[20]J. Barnes and P. Hut, "A hierarchical o (n log n) force-calculation algorithm," Nature **324**, 446–449 (1986).

[21]W. Dehnen, "A very fast and momentum-conserving tree code," The Astrophysical Journal Letters **536** (2000).

[22]A. Saadat and B. Khomami, "Computationally efficient algorithms for incorporation of hydrodynamic and excluded volume interactions in brownian dynamics simulations: A comparative study of the krylov subspace and chebyshev based techniques," The Journal of chemical physics **140**, 184903 (2014).

[23]D. C. Morse, "Theory of constrained brownian motion," Advances in Chemical Physics **128**, 110 (2004).

[24]D. Petera and M. Muthukumar, "Brownian dynamics simulation of beadrod chains under shear with hydrodynamic interaction," The Journal of Chemical Physics **111**, 7614 (1999).

[25]S. Liu, B. Ashok, and M. Muthukumar, "Brownian dynamics simulations of bead-rod-chain in simple shear flow and elongational flow," Polymer **45**, 1383–1389 (2004).

[26]I. M. Neelov, D. B. Adolf, A. V. Lyulin, and G. R. Davies, "Brownian dynamics simulation of linear polymers under elongational flow: Bead–rod model with hydrodynamic interactions," The Journal of Chemical Physics **117**, 4030–4041 (2002).

[27]H. Sim, B. Khomami, and R. Sureshkumar, "Flowinduced chain scission in dilute polymer solutions: Algorithm development and results for scission dynamics in elongational flow," Journal of Rheology **51**, 1223–1251 (2007).

[28]U. S. Agarwal, R. Bhargava, and R. A. Mashelkar, "Brownian dynamics simulation of a polymer molecule in solution under elongational flow," The Journal of Chemical Physics **108**, 1610–1617 (1998).

[29]A. Rey, J. Freire, and J. de la Torre, "Brownian dynamics simulation of flexible polymer chains with excluded volume and hydrodynamic interactions. a comparison with monte carlo and theoretical results," Polymer **33**, 3477–3481 (1992).

[30]H. Öttinger, *Stochastic processes in polymeric fluids* (Springer Berlin, 1996).

[31]P. Doyle, E. Shaqfeh, and A. Gast, "Dynamic simulation of freely draining flexible polymers in steady linear flows," Journal of Fluid Mechanics **334**, 251–291 (1997).

[32]J. D. Schieber and O. Obasanjo, "On estimating stress in freedraining kramers chain simulations using stochastic filtering," Journal of Non-Newtonian Fluid Mechanics **127**, 89–93 (2005).

[33]D. E. Smith, T. T. Perkins, and S. Chu, "Dynamical scaling of dna diffusion coefficients," Macromolecules **29**, 1372–1373 (1996).

[34]J. S. Hur, E. S. Shaqfeh, H. P. Babcock, D. E. Smith, and S. Chu, "Dynamics of dilute and semidilute dna solutions in the start-up of shear flow," Journal of Rheology **45**, 421 (2001).

[35]J. S. Hur, E. S. Shaqfeh, H. P. Babcock, and S. Chu, "Dynamics and configurational fluctuations of single dna molecules in linear mixed flows," Physical Review E **66**, 011915 (2002).

[36]A. V. Lyulin, D. B. Adolf, and G. R. Davies, "Brownian dynamics simulations of linear polymers under shear flow," The Journal of Chemical Physics **111**, 758–771 (1999).

[37]T. W. Liu, "Flexible polymer chain dynamics and rheological properties in steady flows," The Journal of Chemical Physics **90**, 5826–5842 (1989).

[38]J. Hur, E. Shaqfeh, and R. Larson, "Brownian dynamics simulations of single dna molecules in shear flow," Journal of Rheology **44**, 713–742 (2000).

[39]E. S. Shaqfeh, "The dynamics of single-molecule dna in flow," Journal of Non-Newtonian Fluid Mechanics **130**, 1–28 (2005).

[40]C. Sendner and R. Netz, "Single flexible and semiflexible polymers at high shear: Non-monotonic and non-universal stretching response," The European Physical Journal E **30**, 75–81 (2009).

[41]I. Dalal, N. Hoda, and R. Larson, "Multiple regimes of deformation in shearing flow of isolated polymers," Journal of Rheology **56**, 305–332 (2012).

[42]I. S. Dalal, C.-C. Hsieh, A. Albaugh, and R. G. Larson, "Effects of excluded volume and hydrodynamic interactions on the behavior of isolated bead-rod polymer chains in shearing flow," AIChE Journal **60**, 1400–1412 (2014).

[43]M. Pasquali and D. C. Morse, "An efficient algorithm for metric correction forces in simulations of linear polymers with constrained bond lengths," The Journal of Chemical Physics **116**, 1834 (2002).